

On the Origin of Chaos in the Belousov-Zhabotinsky Reaction in Closed and Unstirred Reactors

M. A. Budroni¹, M. Rustici² * and E. Tiezzi¹

¹ Dipartimento di Chimica, Università di Siena, Via della Diana 2a, 53100 Siena, Italy

² Dipartimento di Chimica, Università di Sassari and INSTM, Via Vienna 2, 07100 Sassari, Italy

Abstract. We investigate the origin of deterministic chaos in the Belousov–Zhabotinsky (BZ) reaction carried out in closed and unstirred reactors (CURs). In detail, we develop a model on the idea that hydrodynamic instabilities play a driving role in the transition to chaotic dynamics. A set of partial differential equations were derived by coupling the two variable Oregonator–diffusion system to the Navier–Stokes equations. This approach allows us to shed light on the correlation between chemical oscillations and spatial–temporal dynamics. In particular, numerical solutions to the corresponding reaction-diffusion-convection (RDC) problem show that natural convection can change the evolution of the concentration distribution as well as oscillation patterns. The results suggest a new way of perceiving the BZ reaction when it is conducted in CURs. In conflict with the common experience, chemical oscillations are no longer a mere chemical process. Within this framework the evolution of all dynamical observables are demonstrated to converge to the regime imposed by the RDC coupling: chemical and spatial–temporal chaos are genuine manifestations of the same phenomenon.

Key words: chemical chaos, spatial–temporal chaos, reaction–diffusion–convection system, Belousov–Zhabotinsky reaction

AMS subject classification: 37G35, 35B36, 35Q35

*Corresponding author. E-mail: rustici@uniss.it

1. Introduction

The Belousov-Zhabotinsky (BZ) reaction [1] is the best known non-linear oscillating reaction in homogeneous phase. In spite of its apparent simplicity, the reaction has inspired a huge literature [2] due to the striking spectrum of complex dynamics it can exhibit. In this context the emergence of chemical chaos has attracted primary interest. Instability scenarios by which the BZ dynamics is driven to chaotic oscillations have been detected and studied for open and stirred reactors (Continuous-flow Stirred Reactors, CSTRs). The control of the transition in CSTRs is purely kinetic and correlated to the temperature, the reactant inflow concentration and the mean residence time of the species in the reactor (see the monograph by S. Scott [2] for an extensive discussion). Similarly, kinetic dependences have been shown in affine studies carried out on closed unstirred reactors (CURs) [3, 4], where a chaotic transient was found to occur following a Ruelle-Takens-Newhouse (RTN) scenario [5, 6].

Involving spatial-temporal breaks of symmetry, the BZ reaction in CURs deserves a specific discussion. Self-organized formation of characteristic patterns (typically traveling waves) is the fascinating result of the coupling between kinetics and transport phenomena [7, 8, 9, 10, 11]. Here experimental observations agree with theoretical studies to assume hydrodynamic instabilities as the main responsible for the transition to spatial-temporal chaos. After experimental evidence, the interplay of the kinetics with transport phenomena has been also invoked to explain the onset of chemical chaos. This hypothesis was confirmed by the strict dependence of the transition on *(i)* stirring [5], *(ii)* viscosity [12, 13], *(iii)* the temperature [4] and *(iv)* the reactor geometry [14]. We aim to fill a literature blank existing between the temporal and spatial-temporal approaches to these systems. In details, we shall deal with the following subtle problems: are chemical and spatial-temporal chaos manifestations of the same phenomenon? Or, in other words, does chemical chaos imply spatial-temporal chaos? And, indeed, is the interplay between chemical and transport phenomena instabilities the general origin of chaos for these systems?

The questions are nothing conceptually trivial. They infer a leading role of the transport phenomena in the evolution of a chemical process, whereas a pure chemical description of the kinetics is not capable to explain the transition to complex oscillations. Moreover it implies a not obvious equivalence between mean-field dynamical observables (the spatial averaged concentration of the reaction intermediates) and local dynamical observables (spatial-temporal organization of traveling waves). In the following numerical approach we can verify that the RDC-coupling actually governs the system, driving it to chaos. In this sense chemical and spatial-temporal complexity are different facets of the same phenomenon.

2. The Model

The system is modeled on the basis of the experimental speculations discussed in the introduction. To be more precise, we assume the direct transition to chemical chaos to occur in the far from the equilibrium branch, where the major reactant consumption can be neglected (*pool chemical approximation* [2]). Here the hydrodynamic instabilities present primary influence and the direct

route to chaos can be described by increasing the parameter controlling the velocity field.

2.1. Reaction–Diffusion–Convection (RDC) Equations and Numerical Methods

Consider a two dimensional (\hat{x}, \hat{y}) vertical slab, in which the gravitational field is directed along the \hat{y} vertical axis. A set of partial differential equations is derived by coupling a reaction–diffusion (RD) system [15] to the convection by the Navier-Stokes equations. The set of partial differential equations, formulated in the Boussinesq approximation and written in the vorticity – stream function $(\omega - \psi)$ form, is conveniently non-dimensionalized by using the time scale $t_o = 21 \text{ sec}$ (Oregonator time unit, O.t.u.) and the space scale $x_o = 0.06 \text{ cm}$. Since it has been demonstrated that thermal gradients are negligible with respect to the concentration gradient for the onset of convection [16, 10], the hydrodynamic equations are formulated in the isothermal hypothesis. The resulting model is:

$$\frac{\partial c_i}{\partial t} + D_\nu \left(u \frac{\partial c_i}{\partial x} + v \frac{\partial c_i}{\partial y} \right) - D_i \nabla^2 c_i = k_i(c_1, c_2) \quad i = 1, 2 \quad (2.1)$$

$$\frac{\partial \omega}{\partial t} + D_\nu \left(u \frac{\partial \omega}{\partial x} + v \frac{\partial \omega}{\partial y} \right) - D_\nu \nabla^2 \omega = -D_\nu \sum_i Gr_i \frac{\partial c_i}{\partial x} \quad (2.2)$$

$$\frac{\partial^2 \psi}{\partial x^2} + \frac{\partial^2 \psi}{\partial y^2} = -\omega \quad (2.3)$$

$$u = \frac{\partial \psi}{\partial y} \quad (2.4)$$

$$v = -\frac{\partial \psi}{\partial x} \quad (2.5)$$

where $k_i(c_1, c_2)$ are the kinetic functions, non–dimensionalized on $t_o = 1/k_0 B = 21 \text{ sec}$. They describe the oscillating behavior of the chemical species c_1 and c_2 , within the Oregonator model [17]:

$$k_1(c_1, c_2) = \frac{dc_1}{dt} = \frac{1}{\epsilon} \left[c_1(1 - c_1) + f c_2 \frac{q - c_1}{q + c_1} \right] \quad (2.6)$$

$$k_2(c_1, c_2) = \frac{dc_2}{dt} = c_1 - c_2 \quad (2.7)$$

c_1 and c_2 identify the dimensionless concentrations of the intermediate species HBrO_2 and Ce^{4+} . They are related to the dimensional ones, C_1 and C_2 , as follows

$$c_1 = 2C_1 \frac{k_4}{k_5 A}; \quad c_2 = C_2 \frac{k_4 k_0 B}{(k_5 A)^2} \quad (2.8)$$

where A , B are the starting reactant dimensional concentrations, respectively $[\text{BrO}_3^-]$ and [Malonic Acid]; k_0, k_4, k_5 are dimensional rate constants describing the fundamental steps of the Oregonator mechanism. The kinetic parameters were set $f = 1.6$ (in order to assure the oscillating regime for the Oregonator model), $q = 2k_3k_4/k_2k_5 = 0.01$ and $\epsilon = k_0B/[H^+]k_5A = 0.005$. $D_\nu = \nu t_0/x_0^2 = 58.50$ is the dimensionless viscosity (ν being the kinematic viscosity set equal to the water viscosity $0.01 \text{ cm}^2/\text{s}$), $D_i = Dt_0/x_0^2 = 0.00350$ is the dimensionless diffusivity (D being the dimensional diffusivity of the two species assumed to be equal to $6 \times 10^{-7} \text{ cm}^2/\text{s}$); $u = U/v_0$ and $v = V/v_0$ are dimensionless horizontal and vertical components of the velocity field and v_0 is the velocity scale x_0/t_0 . $Gr_i = gx_0^3\delta\rho_i/\rho_i\nu^2$ is the Grashof number for the i -th species (g is the gravitational acceleration ($980 \text{ cm}/\text{sec}^2$) and $\delta\rho_i/\rho_i$ is the density variation due to the change of the concentration of the i -th species with respect to a reference value c_{0i}). Experimental measurements, performed by Pojman and Epstein [18] for both Fe^{2+} and Ce^{4+} catalyzed CURs–BZ, revealed that $\delta\rho_i/\rho_i \in (1 \times 10^{-3}, 1 \times 10^{-5})$, depending on the catalyst used. However, an estimation of this quantity is rather uncertain and it is included in Gr_i , which is the control parameter chosen to follow the transition to chaos. Gr_i represents the system susceptibility to generate convective motions in virtue of isothermal density gradients. In our simulations the Grashof numbers for the two species were kept equal to each other.

$\psi(x, y, t)$ is defined as the imaginary part of a complex potential. As defined by equations 2.4 and 2.5, it could usefully be treated as a sort of velocity potential. To be more precise the difference between $\psi(x, y, t)$ values at two different points gives the flux through the line segment connecting them. Moreover equation 2.3 expresses the relation existing between $\psi(x, y, t)$ curvature and the vorticity, ω . In this way minima and maxima of $\psi(x, y, t)$ are related to regions of maximum intensity of fluid rotation.

The initial inhomogeneous configurations were set according to Jahnke et al. [19]. They produce spiral waves:

$$c_1^0 = \begin{cases} 0.8 & \text{if } \theta \in [0, 0.5] \\ c_{1(ss)} & \text{elsewhere} \end{cases}$$

$$c_2^0 = \left(c_{2(ss)} + \frac{\theta}{8\pi f} \right) \times 1.30$$

where $c_{1(ss)} = c_{2(ss)} \approx q(f+1)/(f-1)$ and θ is the polar coordinate angle. As suggested by the experimental results about the influence of the initial concentrations on the onset of chaos [3], the original function for c_2^0 was modulated by the factor 1.30. The choice of a spiral as a starting configuration is arbitrary. After a transient period, the RDC coupling determines in every case the formation of characteristic spiral-like structures. This fact was numerical verified by starting from different configurations (for example gaussian fronts). The equation's system 2.1–2.5 was solved by means of the alternating direction finite difference method over a square grid (100×100 points) and using the integration time step, $ht = 1 \times 10^{-5}$ (tested to be a stable choice). There were imposed no-slip boundary conditions for the fluid velocity and no-flux boundary conditions for chemical concentrations at the slab walls.

3. Numerical Analysis

3.1. The route to chemical chaos

The first point is to verify if the hypothesis assumed in the derivation of the model lead us to a significant agreement with the experimental results.

Both in real and numerical experiments, the time series record chemical species' concentration averaged over the spatial domain. In the case of the real experiment, the spatial domain is defined as the region explored by the spectrophotometric beam which scans the reactor (typically a quartz cuvette). In modern spectrophotometers this domain can be modulated by the user and the length scale x_0 represents a classical setting. The spatial average of the intermediates' absorbance (which is directly related to their concentrations) is reported as a function of the time. Figure 1 illustrates a typical spectrophotometric time series where the oscillations of the catalyst (in this case Ferroin) absorbance show a transient chaotic behavior (see the red box in the Figure). Chemical chaos occurs via a similar Ruelle–Takens–Newhouse scenario, characterized by a finite number of supercritical Hopf bifurcations [20]. Successive regimes defining the route from periodic to chaotic oscillations are framed in different colored boxes. In detail, the blue box encloses the first periodic regime, where an initial stirring hides the emergence of transport phenomena and the dynamics is fully described by the reaction kinetics; the green and the yellow boxes respectively frame the emergence of a periodic regime sustained by the coupling of kinetics with transport phenomena and the quasi-periodic behavior preceding chaos. Technical information on the experimental set-up and a quantitative characterization of this transition can be found in [6].

In our simulations, the spatial averages of the species's concentration, $\langle c_i(x, y, t) \rangle$, are computed over the solving grid and recorded every 1000-time steps. Although physically meaningful values of Gr_i range in the interval $[-400, 400]$, calculations are circumscribed to $Gr_i \in [0.00, 12.50]$, where an affective coupling between kinetics and transport phenomena can be found. In particular, beyond the threshold $Gr_i = 12.50$, the system is forced to an immediate homogenization of the concentration distribution, hindering the formation of self-organized structures. This last condition is related to stirred reactors, whose dynamics is completely imposed by the reaction kinetics. In our approach, each Grashof number's value specifies a transient regime of the experimental route to chaos. Following the bifurcation scenario, various dynamical regimes can be discerned, some of which cannot be detected by the analysis of experimental data. Here we focus on the main regimes which find a qualitative overlapping with the experiment. The route to chemical chaos is characterized by means of the Fast Fourier Transforms (FFTs) of $\langle c_i(x, y, t) \rangle$ and by the reconstruction of the related attractors. In the illustration of the successive attractors as Gr_i is varied, we keep fixed the region representing the phase space. This allows us to better follow the system evolution. *Periodic regimes.* In Figure 2.a we show the time series obtained for the convection-less state: $Gr_i = 0.00$. The corresponding limit cycle (Figure 2.c) is characterized by the fundamental frequency $\omega_0 = 0.742 \text{ O.t.u.}^{-1}$ (Figure 2.b). Compared to the spectrophotometric registration, this regime refers to the initial stage, where the initial stirring of the reactants hinders any macroscopic inhomogeneity and, indeed, the onset of natural convection (see Figure 1, frame I).

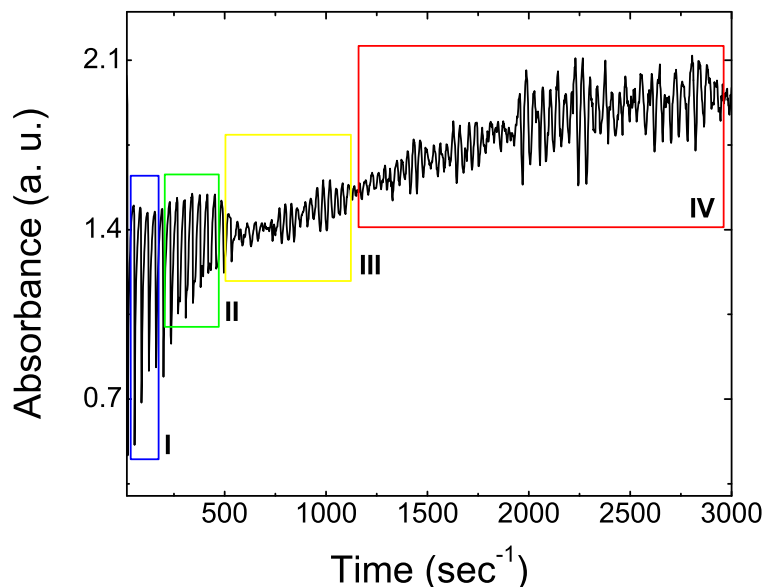


Figure 1: A typical spectrophotometric registration of the BZ reaction carried out in a CUR. The time series describes the oscillations of the catalyst (in this case the Ferriin) absorbance. (Courtesy of Dr. F. Rossi).

The analysis in Figure 3 is related to the numerical solution of the RDC equations for $Gr_i = 5.50$. After a transient period (about 70 O.t.u.), the dynamics of c_1 and c_2 is periodic with the fundamental frequency $\omega_1 = 0.397$ O.t.u.⁻¹ (Figure 3.b), different from that observed in Figure 2.b. The emergence of a new main frequency suggests the effective coupling between the convective contribution and the simple reaction–diffusion system. With reference to the spectrophotometric registration, this regime identifies the final part of the periodic pattern (Figure 1, frame II).

Quasi-periodic regime. As Gr_i assumes the value 9.80, a supercritical Hopf bifurcation to the quasiperiodic regime occurs (see Figure 4). The toroidal nature of the flow in the phase-space (Figure 4.c) is confirmed by the Fourier amplitude spectrum (Figure 4.b). In particular, two characteristic frequencies ($\omega_1 = 0.397$, $\omega_2 = 0.549$) and their linear combinations are pointed out. The bifurcation type can be inferred by the fact that ω_1/ω_2 is an irrational number. This regime is associated to the interval III in Figure 1.

Chaotic regime. For $Gr_i \in [10, 00, 12.50]$, an aperiodic behavior is observed (Figure 5.a). The dynamics of the system in the phase-space is bounded and associated with the strange attractor in Figure 5.d. The time series manifests sensibility to initial conditions consistently with one of the most connotative features of deterministic chaos. The chaotic nature of the dynamics can be inferred also by the FFT amplitude spectrum, which highlights a continuous pattern, with the main contributes at low values. Moreover, we tested for chaos by calculating the largest Lyapunov

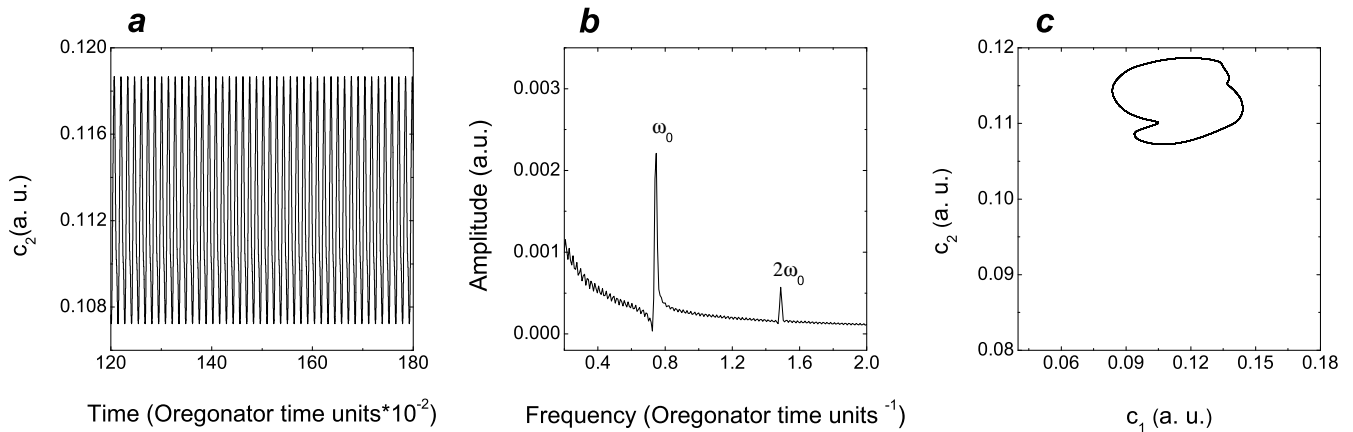


Figure 2: $Gr_i = 0.00$. (a) c_2 time series. (b) Fourier amplitude spectrum: a periodic regime is revealed by the main frequency $\omega_0 = 0.742$ O.t.u. $^{-1}$. (c) The phase space representation shows a limit cycle.

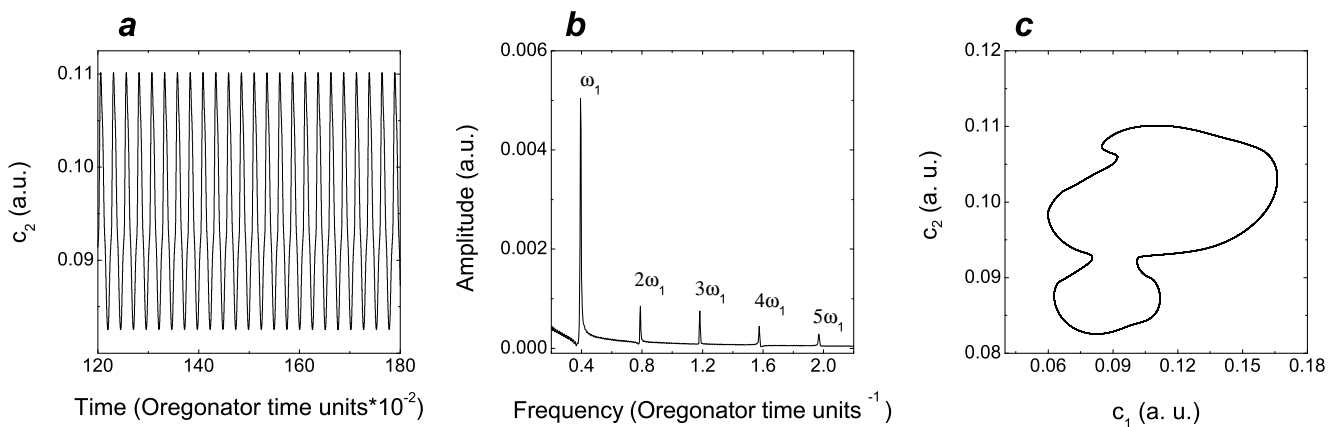


Figure 3: $Gr_i = 5.50$. (a) c_2 time series. (b) Fourier amplitude spectrum: the new periodic regime is characterized by the main frequency $\omega_1 = 0.397$ O.t.u. $^{-1}$. (c) The phase space representation shows the evolution to a new limit cycle.

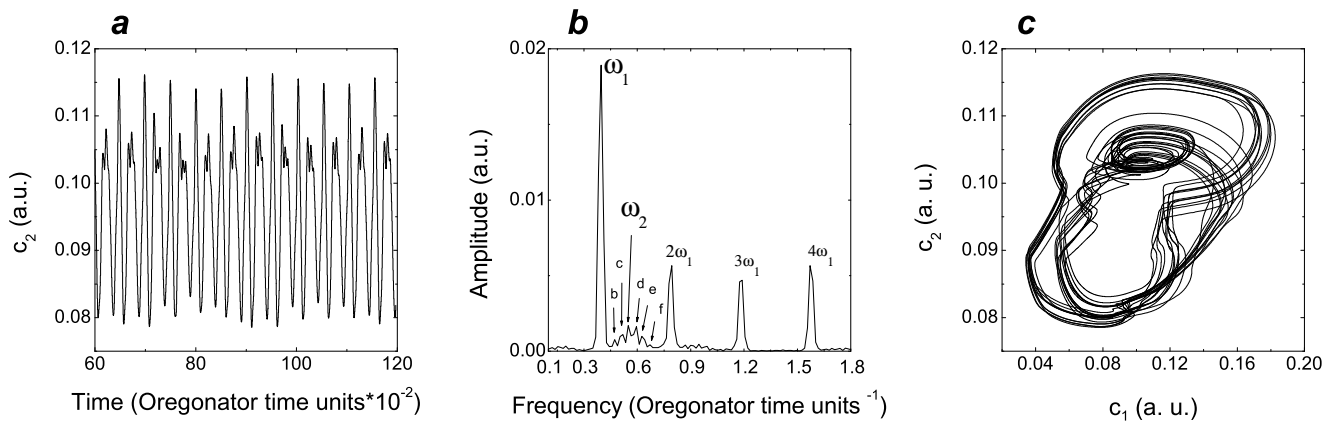


Figure 4: $Gr_i = 9.80$. (a) c_2 time series. (b) Fourier amplitude spectrum: the quasi-periodic regime is identified by the two incommensurable frequencies $\omega_1 = 0.397$ O.t.u. $^{-1}$ and $\omega_2 = 0.549$ O.t.u. $^{-1}$. Some harmonic combinations are shown: $b = 3\omega_2 - 3\omega_1$, $c = 6\omega_2 - 7\omega_1$, $d = \omega_1 + 1/2\omega_1$, $e = 4\omega_2 - 4\omega_1$, $f = 7\omega_2 - 8\omega_1$. (c) The phase space representation shows a bi-dimensional torus T^2 .

exponents. The computation was performed by using the Kantz algorithm from TISEAN package [21, 22] (Figure 5.c). This method looks for exponential perturbation growth by implementing the formula

$$S(\epsilon, m, t) = \left\langle \ln \left(\frac{1}{U_n} \sum_{s_{n'} \in U_n} |s_{n+t} - s_{n'+t}| \right) \right\rangle_n \quad (3.1)$$

where s'_n represents a return point in the space phase, close to the point s_n visited previously by the system; m is the embedding dimension; U_n the neighborhood with diameter ϵ where the algorithm search for the return point. The maximal Lyapunov exponent λ_1 is given by the slope of the pencil $S(\epsilon, m, t)$ (derived considering different m), where it exhibits a linear increase, identical for each m -curve. A value of $\lambda_1 \approx 0.019$ was found by a linear regression of the curves in the region between 0 and 40 iterations n .

This regime corresponds to the frame IV in Figure 1.

3.2. The route to spatial-temporal chaos

What about spatial-temporal dynamics of the chemical waves when Gr_i assumes the considered sequence of values?

To address this question we can use the method and the results in [23]. For the sake of clarity we recall the main features in it.

The idea was to monitor the evolution of the spiral structures in terms of the tip dynamics, assuming it describes unambiguously the spiral evolution. The tip position, $\mathbf{x}_{tip}(t) = (x_{tip}(t), y_{tip}(t))$, is

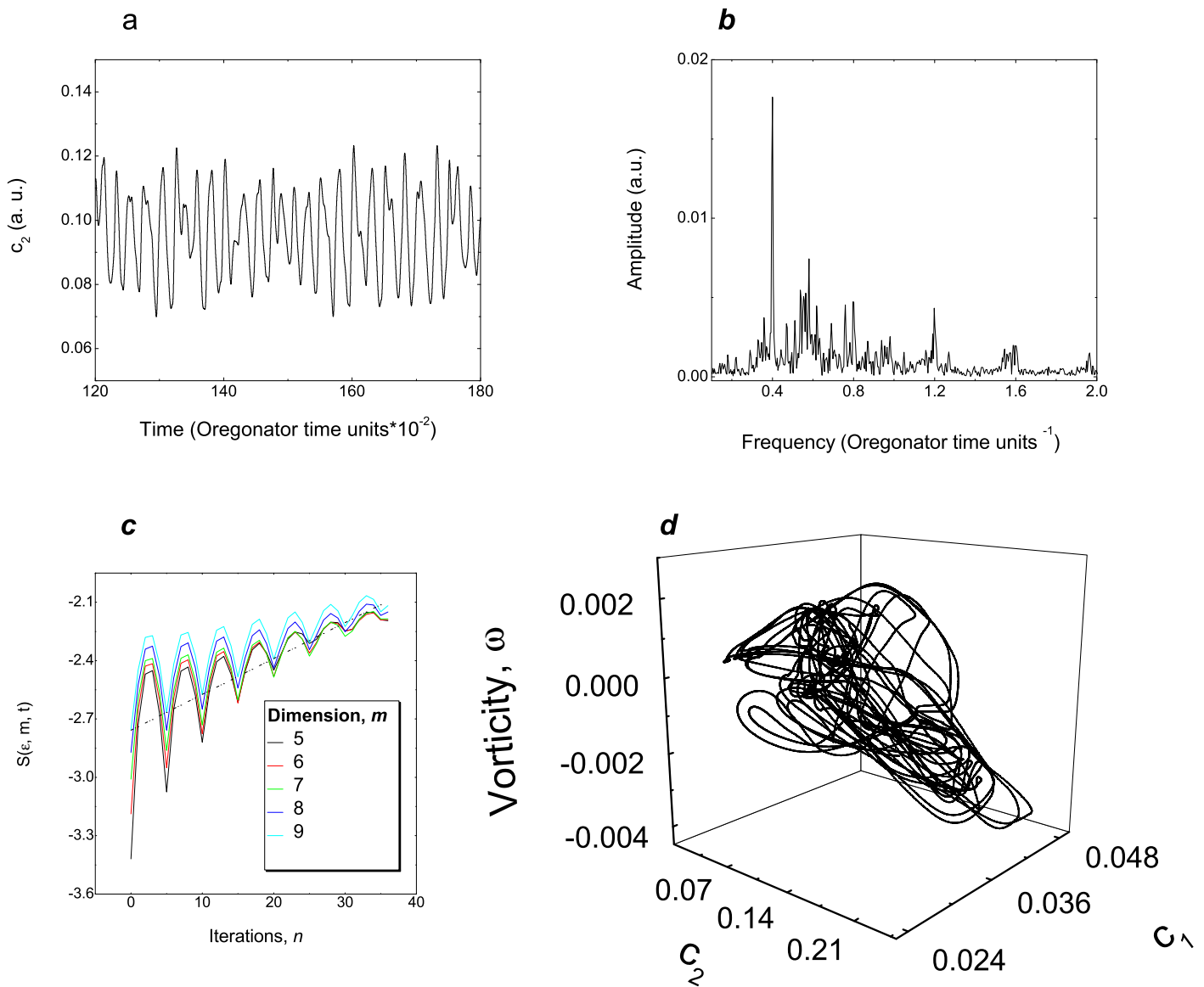


Figure 5: $Gr_i = 12.50$. (a) c_2 time series. (b) Fourier amplitude spectrum: the chaotic regime can be inferred by the continuous spectrum of frequencies. (c) Computation of the maximum exponent by the Kantz algorithm. The value of $\lambda_1 \approx 0.019$ is obtained by the linear regression of the curves for $m \in 5 \div 7$, in the zone $n \in [0, 40]$ iterations. (d) The phase space representation shows a strange attractor.

analytically defined as the point of the spatial domain where the cross product between the gradient vectors of c_1 and c_2 , is maximal [19]:

$$(\nabla c_1 \times \nabla c_2)_{x_{tip}, y_{tip}} = \sup\{(\nabla c_1 \times \nabla c_2)_{i,j} \forall i, j\} \quad (3.2)$$

where i, j are the integer coordinates of the solving grid.

When the convective contribution in the system is significant high, the definition given in equation 3.2 may lose its unambiguous meaning due to distortions and possible breaks of the spiral wave. To identify the tip position additional assumptions were considered:

1. The tip belongs to the main arm of the spiral. The lifetime of the concentration “islands” produced by the spiral breaks is short, hinting that their role in the spiral evolution can be ignored;
2. Continuity to the position of the spiral tip in the previous time step. Apart for limited time intervals during which spiral breaks, the tip follows a continuous trajectory and, at each time step, it has high probability to be found close to its previous position.
3. Contiguity to the $\psi(x, y, t)$ minimum closer to the spiral. As we showed [23], the $\psi(x, y, t)$ minima exert an attracting power on the tip and, in absence of $\psi(x, y, t)$ maxima, drives its evolution. In this way $\psi(x, y, t)$ minima are useful to detect the tip position in presence of spiral distortions and breaks.

In view of the second goal of the present work (demonstrating the equivalence between mean-field and local observables), this method allows us a quali-quantitative comparison between the transition to chemical and spatio-temporal chaos. The tip observable used to derive time series from spatial-temporal dynamics is $d_{tip}(t) = |\mathbf{x}_{tip}(t)|$. We characterize the emerging regimes by means of FFTs. The spatial patterns traced by the tip are also illustrated.

$Gr_i \in [0.00, 5.50)$. The system corresponds to a simple reaction-diffusion model. In this regime the hydrodynamic influence on spiral structures is absent: any distortions or breaks-down can be detected. The spiral tip localization reflects the traditional definition in equation 3.2 and the resulting tip trace describes a quasi-periodic spatial-temporal regime. This is revealed by the two main incommensurable frequencies, $\alpha_1 = 0.747$ O.t.u.⁻¹ and $\alpha_2 = 1.071$ O.t.u.⁻¹ (Figure 6.b). The nature of the dynamics is not surprising, since it is very close to what was found in Ref. [19], where f was used as a control parameter in a simple RD system. This regime is protracted for Gr_i ranging up to 5.50. Within this entire interval, the tip dynamics and the spiral structures do not appreciably suffer of the weak hydrodynamic field and the characteristic frequencies differ in a negligible way from what is found for $Gr_i = 0.00$.

$Gr_i \in [5.50, 9.80)$. The spirals are distorted by the velocity field, but not yet object to any breaking phenomena. Within this hydrodynamic conditions, it can be recognized the rising of the disturbing action of the velocity field. Nevertheless the tip dynamics describes a periodic regime. The trajectory follows a closed cycle, characterized by the main frequency $\alpha_3 = 0.397$ O.t.u.⁻¹. The transformation occurring in the pattern type is concomitant with the emergence of an effective

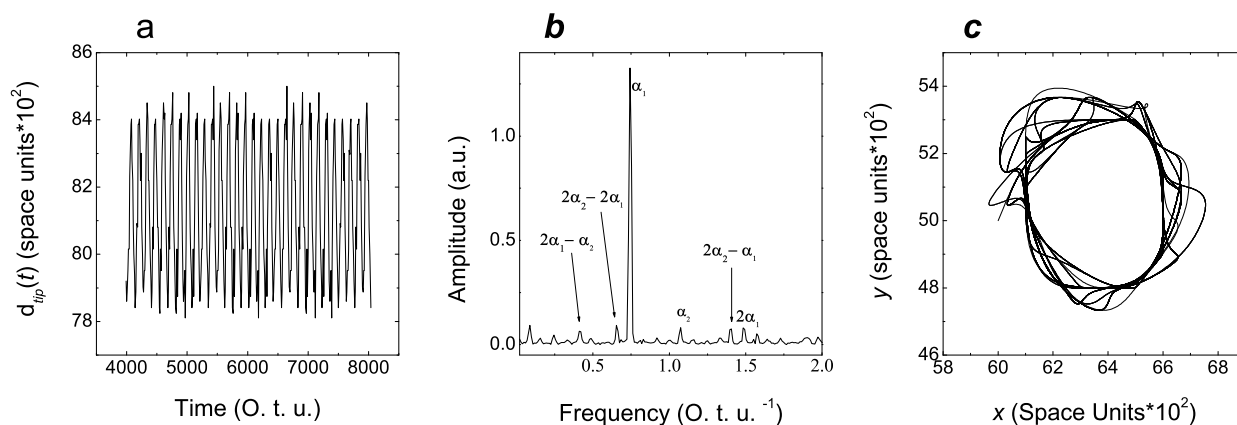


Figure 6: $Gr_i = 0.00$. (a) $d_{tip}(t)$ time series. (b) FFT amplitude spectrum of $d_{tip}(t)$. A quasi-periodic regime is detected by the two incommensurable frequencies $\alpha_1 = 0.747$ O.t.u.⁻¹ and $\alpha_2 = 1.071$ O.t.u.⁻¹. The harmonic combinations are reported in the figure. (c) Spiral tip trajectory.

RDC coupling and the production of characteristic RDC-structures. The reduction in the absolute value of the main frequency (0.747 to 0.397 O.t.u.⁻¹) is associated to the hydrodynamic resistance, which cannot be neglected any more (Figure 7).

$Gr_i \in [9.80, 10, 00)$. The spiral tip dynamics grows in complexity. The topological study in [23] has outlined the correlation between the tip motion and $\psi(x, y, t)$ minima and maxima. After that, it was possible to classify the action exerted by these pseudo-potentials on a chemical wave and to understand the mechanism by which complexity in tip trajectory arises. Here we directly report the FFT amplitude spectrum of $d_{tip}(t)$ for $Gr_i = 9.80$ (see Figure 8.b). This points out the presence of a Hopf bifurcation, characterized by the emergence of a new frequency ($\alpha_4 = 0.549$ O.t.u.⁻¹), whose ratio to the main one, α_3 , is an irrational number. The harmonic combinations of the two main frequencies are also shown.

$Gr_i \in [10.00, 12.50]$. The convective forcing hinders the persistence of spiral-like waves. The structures are broken into many residuals and are strongly distorted. The trajectory traced by the tip is reminiscent of a random-walk (Figure 9.c), resulting in an aperiodic time series (Figure 9.a). Both the analysis of the maximal Lyapunov exponent (which presents a positive value equal to 0.2413 ± 0.0082 , (Figure 10) and the FFT's analysis (which highlights an amplitude spectrum with an infinite number of frequencies (Figure 9.b)), clearly confirm the chaotic nature of the dynamics.

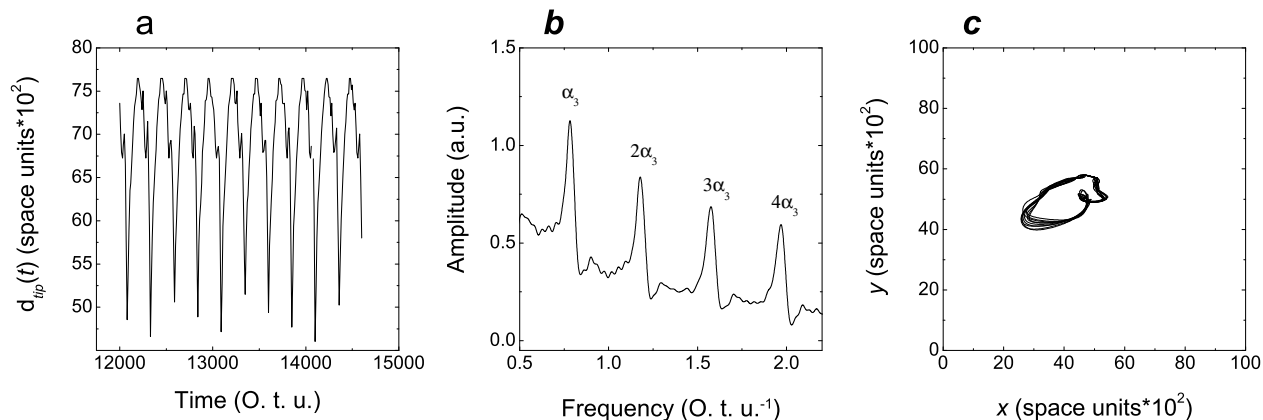


Figure 7: $Gr_i = 5.50$. (a) $d_{tip}(t)$ time series. (b) FFT amplitude spectrum of $d_{tip}(t)$. The main frequency $\alpha_3 = 0.397$ O.t.u. $^{-1}$ characterizes the periodic regime. (c) Spiral tip trajectory.

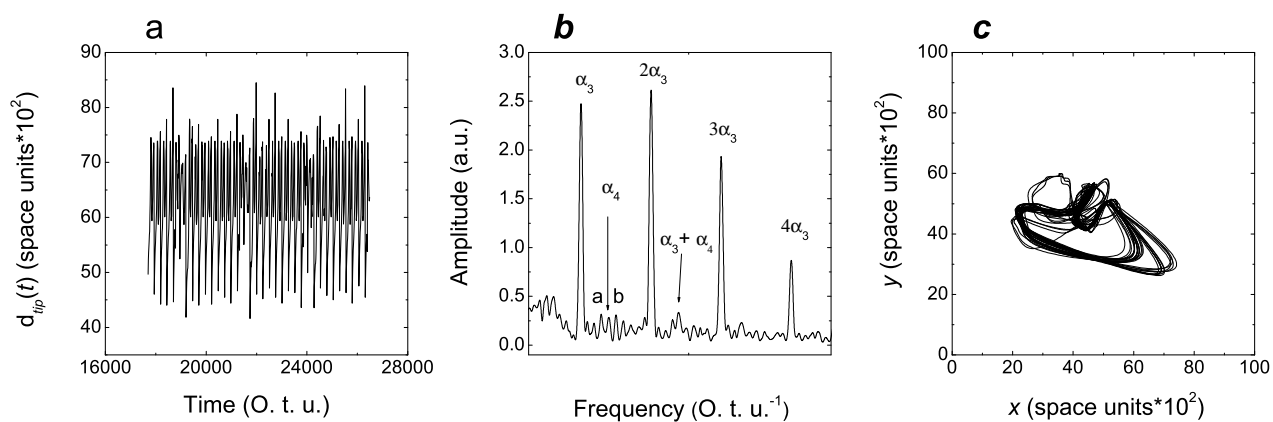


Figure 8: $Gr_i = 9.80$. (a) $d_{tip}(t)$ time series. (b) FFT amplitude spectrum of $d_{tip}(t)$. A quasi-periodic regime is detected by the two incommensurable frequencies: $\alpha_3 = 0.397$ O.t.u. $^{-1}$ and $\alpha_4 = 0.549$ O.t.u. $^{-1}$. The harmonic combination shown are: $\alpha_3 + \alpha_4$, $a = 6\alpha_4 - 7\alpha_3$, $b = \alpha_4 + 1/2\alpha_3$. (c) Spiral tip trajectory.

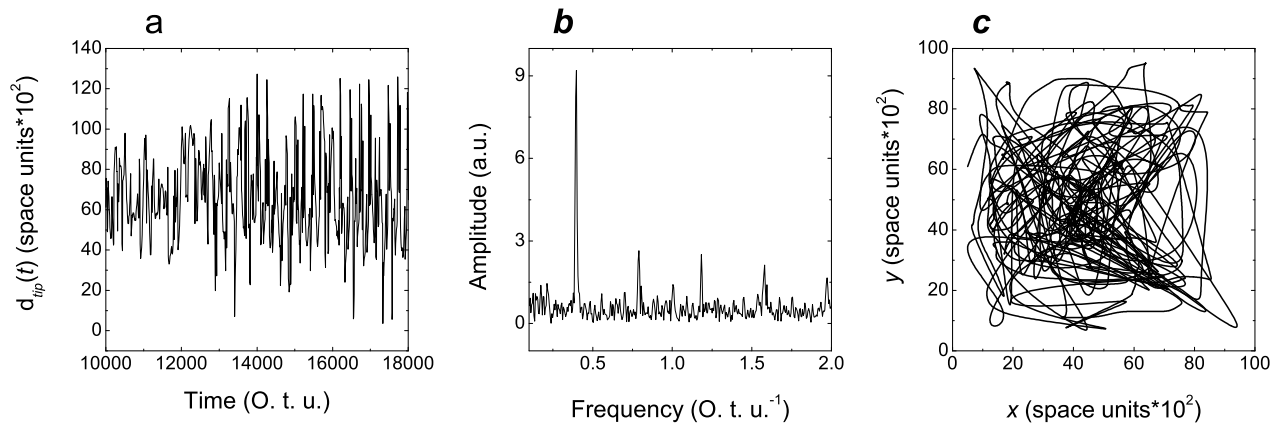


Figure 9: $Gr_i = 12.10$. (a) $d_{tip}(t)$ time series. (b) FFT amplitude spectrum of $d_{tip}(t)$. The chaotic regime can be inferred by the continuous spectrum of frequencies. (c) Spiral tip trajectory.

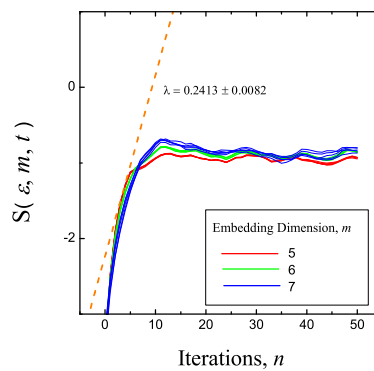


Figure 10: Computation of the maximal Lyapunov exponent by the Kantz algorithm. The value of $\lambda = 0.2413 \pm 0.0082$ is obtained by the linear regression of the curves $m = 5 - 7$, in the zone between 2 - 5 iterations.

Gr_i	Properties	Regimes	Characteristic Values
$0.00 \leq Gr_i < 5.50$			
	$d_{tip}(t)$	Quasi-Periodic	$\alpha_1 = 0.747, \alpha_2 = 1.071$
	$\langle c_i(x, y, t) \rangle$	Periodic	$\omega_0 = 0.742$
$5.50 \leq Gr_i < 9.80$			
	$d_{tip}(t)$	Periodic	$\alpha_3 = 0.397$
	$\langle c_i(x, y, t) \rangle$	Periodic	$\omega_1 = 0.397$
$9.80 \leq Gr_i < 10.00$			
	$d_{tip}(t)$	Quasi-Periodic	$\alpha_3 = 0.397, \alpha_4 = 0.549$
	$\langle c_i(x, y, t) \rangle$	Quasi-Periodic	$\omega_1 = 0.397, \omega_2 = 0.549$
$10.00 \leq Gr_i \leq 12.50$			
	$d_{tip}(t)$	Chaotic	$\lambda_1 = 0.2413$
	$\langle c_i(x, y, t) \rangle$	Chaotic	$\lambda = 0.0189$

Table 1: Dynamical regimes and characteristic values describing the evolution of $\langle c_i(x, y, t) \rangle$ and $d_{tip}(t)$.

4. Discussion

The main aim of this paper was to understand the origin and the nature of the chaos experimentally observed in BZ–CURs. The problem was defined by the two fundamental questions: is the RDC coupling the source of chemical and spatial–temporal chaos? Does spatial–temporal chaos imply chemical chaos?

The results of the analysis are systematically reported in table 1. The first conclusion we can draw is that actually a transition process from periodic to chaotic oscillations is induced by hydrodynamic instabilities. We showed this fact by increasing the control parameter in the range $Gr_i \in [0.00, 12.50]$. In agreement with experimental results, chaos occurs following a similar Ruelle-Takens-Newhouse scenario characterized by three successive supercritical Hopf bifurcations. The Gr_i critical points are 5.50, 9.80 and 10.00. A spatial–temporal approach allows us to appreciate the complexity emerging as Gr_i is increased [23]. It is hidden and not deductible by a purely kinetic analysis. Within the range $Gr_i \in [5.50, 12.50]$, the coupling between kinetics and transport phenomena gives rise to self–sustained structures, the RDC patterns. These are spiral–like traveling waves, whose structure and dynamics are mainly determined by the mutual feed–back between the wave itself and the velocity field. The convective instabilities observed diverge from a Rayleigh–Bénard type problem. Here the spatial–temporal breaks of symmetry are induced by the non–linear and dynamical organization of chemical inhomogeneities instead than a static linear gradient of concentration. As discussed in topological terms in [23], the range $Gr_i \in [5.50, 12.50]$ is suitable for observing the transition to spatial–temporal chaos. Beyond the

threshold, $Gr_i = 12.50$, the system is forced to an immediate homogenization of the concentration distribution, hindering the formation of any self-organized structure. This condition simulates stirred reactors, whose dynamics is completely imposed by the reaction kinetics.

The comparison between $\langle c_i(x, y, t) \rangle$ and $d_{tip}(t)$ provides a meaningful answer to the second initial question. A surprising congruence between the two transition scenarios is found, both under a qualitative and a quantitative profile. As a matter of fact, also the spatial-temporal route to chaos follows a similar RTN scenario. Apart for Gr_i ranging between 0.00 and 5.50 (where the RDC coupling is negligible), equivalent bifurcation points introduce to correspondent regimes. Precisely, the characteristic values (FFTs frequencies) describing the dynamical regimes are the same. The results demonstrate that the RDC-coupling plays a leading role in the BZ reaction in CURs and is at the origin both of chemical and spatial-temporal chaos. Depending on the strength with which the RDC-interplay occurs, specific regimes are imposed to the system and all dynamical observable evolve coherently. Such a congruence is numerically proved both for mean and local quantities, driving us to the deeper conclusion that CURs-BZ oscillations cannot be considered a mere chemical process, but rather a reaction-diffusion-convection process. In this sense chemical and spatial-temporal chaos are genuine manifestations of the same phenomenon, and the former cannot be explained without spatial-temporal instabilities. Experimental studies are in progress as a further confirmation of our results.

Acknowledgements

We acknowledge Prof. Vitaly Volpert and Dr. Marco Masia for their invaluable contribution to the initial part of this project. This work makes use of results produced by the Cybersar Project managed by the Consorzio COSMOLAB, a project co-funded by the Italian Ministry of University and Research (MIUR) within the Programma Operativo Nazionale 2000-2006 “Ricerca Scientifica, Sviluppo Tecnologico, Alta Formazione” per le Regioni Italiane dell’Obiettivo 1 (Campania, Calabria, Puglia, Basilicata, Sicilia, Sardegna) - Asse II, Misura II.2 “Società 340 dell’Informazione”, Azione a “Sistemi di calcolo e simulazione ad alte prestazioni”. More information is available at <http://www.cybersar.it>.

References

- [1] A. M. Zhabotinsky. *Periodical oxidation of malonic acid in solution (a study of the Belousov reaction kinetics)*. Biofizika, 9 (1964), 306–11.
- [2] S. K. Scott. *Chemical Chaos*. Oxford University Press, Oxford, 1993.
- [3] G. Biosa, M. Masia, N. Marchettini, M. Rustici. *A ternary nonequilibrium phase diagram for a closed unstirred Belousov-Zhabotinsky system*. Chem. Phys., 308 (2005), No. 1–2, 7–12.

- [4] M. Masia, N. Marchettini, V. Zambrano, M. Rustici. *Effect of temperature in a closed unstirred Belousov-Zhabotinsky system*. Chem. Phys. Lett., 341 (2001), No. 3–4, 285–291.
- [5] M. Rustici, M. Branca, C. Caravati, E. Petretto, N. Marchettini. *Transition scenarios during the evolution of the Belousov-Zhabotinsky reaction in an unstirred batch reactor*. J. Phys. Chem., 103 (1999), No. 33, 6564–6570.
- [6] F. Rossi, M. A. Budroni, N. Marchettini, L. Cutietta, M. Rustici, M. L. Turco Liveri. *Chaotic dynamics in an unstirred ferroin catalyzed Belousov-Zhabotinsky reaction*. Chem. Phys. Lett., 480 (2009), No. 4–6, 322–326.
- [7] M. C. Cross, P. C. Hohenberg. *Pattern formation outside of equilibrium*. Rev. Mod. Phys., 65 (1993), No. 3, 851–1124.
- [8] A. Abramian, S. Vakulenko, V. Volpert (Eds). *Patterns and waves*. AkademPrint, Saint Petersburg, 2003.
- [9] Y. Wu, D. A. Vasquez, B. F. Edwards, J. W. Wilder. *Convective chemical-wave propagation in the Belousov-Zhabotinsky reaction*. Phys. Rev. E, 51 (1995), No. 2, 1119–1127.
- [10] J. W. Wilder, B. F. Edwards, D. A. Vasquez. *Finite thermal diffusivity at the onset of convection in autocatalytic systems: Continuous fluid density*. Phys. Rev. A, 45 (1992), No. 4, 2320–2327.
- [11] K. I. Agladze, V. I. Krinsky, A. M. Pertsov. *Chaos in the non-stirred Belousov-Zhabotinsky reaction is induced by interaction of waves and stationary dissipative structures*. Nature, 308 (1984), 834–835.
- [12] N. Marchettini, M. Rustici. *Effect of medium viscosity in a closed unstirred Belousov-Zhabotinsky system*. Chem. Phys. Lett., 317 (2000), No. 6, 647–651.
- [13] F. Rossi, F. Pulselli, E. Tiezzi, S. Bastianoni, M. Rustici. *Effects of the electrolytes in a closed unstirred Belousov-Zhabotinsky medium*. Chem. Phys., 313 (2005), 101–106.
- [14] M. L. Turco Liveri, R. Lombardo, M. Masia, G. Calvaruso, M. Rustici. *Role of the Reactor Geometry in the Onset of Transient Chaos in an Unstirred Belousov-Zhabotinsky System*. J. Phys. Chem. A, 107 (2003), No. 24, 4834–4837.
- [15] R. Kapral, K. Showalter. *Chemical waves and patterns*. Kluwer Academic Publisher, Dordrecht/Boston/London, 1995.
- [16] K. A. Cliffe, S. J. Taverner, H. Wilke. *Convective effects on a propagating reaction front*. Phys. Fluids, 10 (1998), No. 3, 730–741.
- [17] R. J. Field, M. Burger. *Oscillations and travelling waves in chemical systems*. Wiley, New York, 1985.

- [18] J. A. Pojman, I. Epstein. *Convective effects on chemical waves. I.: Mechanisms and stability criteria*. J. Phys. Chem., 94 (1990), 4966–4972.
- [19] W. Jahnke, W. E. Skaggs, A. T. Winfree. *Chemical vortex dynamics in the Belousov–Zhabotinsky reaction and in the two–variable Oregonator model*. J. Phys. Chem., 93 (1989), No. 2, 740–749.
- [20] S. Newhouse, D. Ruelle, F. Takens. *Occurrence of strange axiom A attractors near quasiperiodic flows on T^m ($m = 3$ or more)*. Commun. Math. Phys., 64 (1978), 35.
- [21] H. Kantz, T. Schreiber. *Nonlinear time series analysis*. Cambridge University Press, Cambridge, 1997.
- [22] The TISEAN software package is publicly available at <http://www.mpiik-sdresden.mpg.de/~TISEAN>.
- [23] M. A. Budroni, M. Masia, M. Rustici, N. Marchettini, V. Volpert. *Bifurcations in spiral tip dynamics induced by natural convection in the Belousov–Zhabotinsky reaction*. J. Chem. Phys., 130 (2009), No. 2, 024902-1–8.